

NiMark: A Non-intrusive Watermarking Framework against Screen-shooting Attacks

Yufeng Wu¹, Xin Liao¹, Baowei Wang², Han Fang³, Xiaoshuai Wu¹ and Guiling Wang⁴

¹College of Cyber Science and Technology, Hunan University

²School of Computer Science, Nanjing University of Information Science and Technology

³School of Computing, National University of Singapore

⁴Department of Computer Science, New Jersey Institute of Technology

wuyufeng0523@163.com, xinliao@hnu.edu.cn, wbw.first@163.com, fanghan@nus.edu.sg, shinewu@hnu.edu.cn, gwang@njit.edu

Abstract

Unauthorized screen-shooting poses a critical data leakage risk. Resisting screen-shooting attacks typically requires high-strength watermark embedding, inevitably degrading the cover image. To resolve the robustness-fidelity conflict, non-intrusive watermarking has emerged as a solution by constructing logical verification keys without altering the original content. However, existing non-intrusive schemes lack the capacity to withstand screen-shooting noise. While deep learning offers a potential remedy, we observe that directly applying it leads to a previously underexplored failure mode, the Structural Shortcut: networks tend to learn trivial identity mappings and neglect the image-watermark binding. Furthermore, even when logical binding is enforced, standard training strategies cannot fully bridge the noise gap, yielding suboptimal robustness against physical distortions. In this paper, we propose NiMark, an end-to-end framework addressing these challenges. First, to eliminate the structural shortcut, we introduce the Sigmoid-Gated XOR (SG-XOR) estimator to enable gradient propagation for the logical operation, effectively enforcing rigid image-watermark binding. Second, to overcome the robustness bottleneck, we devise a two-stage training strategy integrating a restorer to bridge the domain gap caused by screen-shooting noise. Experiments demonstrate that NiMark consistently outperforms representative state-of-the-art methods against both digital attacks and screen-shooting noise, while maintaining zero visual distortion.

1 Introduction

The illicit capture of displayed content via external cameras constitutes a severe threat to information security. Digital watermarking has long served as a fundamental defense mechanism for identifying ownership and tracing leakage sources. However, unlike lossless digital transmission, this process introduces complex distortions like Moiré patterns and lightness distortion [Fang *et al.*, 2018; Wengrowski

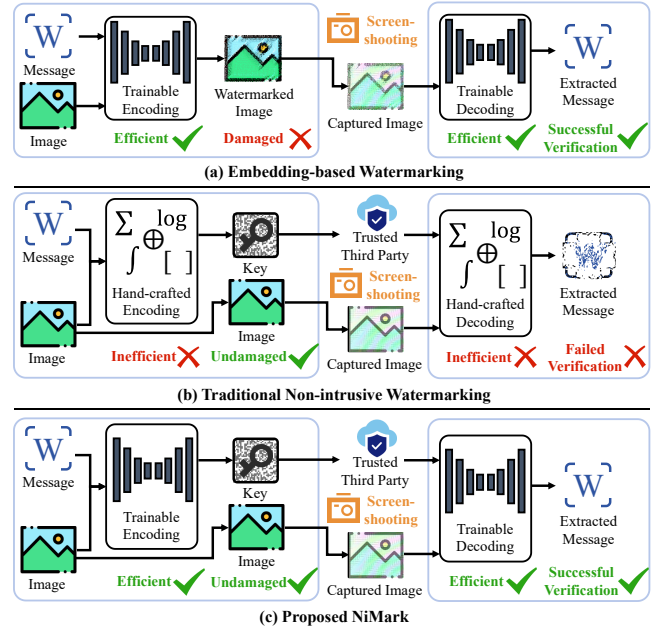


Figure 1: Comparison of different watermarking frameworks against screen-shooting attacks. (a) Embedding-based Watermarking: Although robust against screen-shooting, it inevitably degrades the cover image quality by explicitly modifying pixel values. (b) Traditional Non-intrusive Watermarking: While preserving the original image, it fails to resist the severe distortions caused by screen-shooting due to the limited robustness of hand-crafted features. (c) Proposed NiMark: By harnessing the powerful capability of deep learning, our framework achieves strong robustness against screen-shooting attacks within a non-intrusive architecture, guaranteeing zero visual distortion.

and Dana, 2019], rendering most conventional watermarking schemes ineffective. Current solutions predominantly rely on embedding-based watermarking [Tancik *et al.*, 2020; Fang *et al.*, 2022; Li *et al.*, 2024]. While robust, these methods inevitably degrade visual quality by modifying pixel values (Fig. 1(a)). In high-security applications requiring strict data integrity, such modifications are prohibitive, necessitating non-intrusive alternatives.

To circumvent the fidelity-robustness trade-off, non-

intrusive watermarking, also known as zero-watermarking [Wen *et al.*, 2003], has emerged as a vital research direction. Fig. 1(b) depicts this approach, where instead of modifying the image, the algorithm extracts essential features and logically combines them with the copyright message to construct a verification key. However, the current state of non-intrusive watermarking research faces a significant bottleneck. The vast majority of existing schemes still rely on traditional, hand-crafted algorithms. These manual feature extractors are designed based on prior knowledge of signal processing and lack the adaptive capacity to capture deep, semantic features resilient to the severe non-linear distortions of screen-shooting. Consequently, as shown in the middle row of Fig. 1, traditional methods often fail to verify copyright under real-world screen-shooting attacks.

Conversely, while deep neural networks have revolutionized image processing, an end-to-end deep learning framework for robust non-intrusive watermarking remains a virtually untouched domain. In exploring this uncharted territory, we identify a critical obstacle, the Structural Shortcut. Non-intrusive watermarking necessitates a strong binding between the cover image and the copyright message. However, enforcing this dependency in a deep learning framework is challenging. Lacking a mechanism to enforce logical binding, the network may converge to a degenerate solution that largely neglects the image features and instead approximates a trivial identity mapping. Crucially, if the key becomes a self-contained carrier independent of the image, the copyright binding is severed, undermining the protection mechanism.

Furthermore, even if the structural shortcut is averted, a secondary challenge persists: the Noise Domain Gap. Simultaneously optimizing for logical binding and resistance to screen-shooting complicates the learning process. Standard training strategies cannot fully bridge the domain gap, resulting in suboptimal robustness against real-world noise.

To address these challenges, we propose NiMark, the first end-to-end deep learning framework tailored for screen-shooting resistant non-intrusive watermarking, as visualized in Fig. 1(c). Unlike previous approaches, NiMark utilizes deep neural networks to ensure robustness while guaranteeing zero visual distortion. Our methodology is designed to mitigate the structural shortcut and achieve robustness through model construction and a tailored training strategy.

First, drawing inspiration from traditional non-intrusive schemes, we identify the logical XOR operation as the essential constraint for binding the image features and the watermark. To integrate this discrete logic into a deep learning framework, we propose the Sigmoid-Gated XOR (SG-XOR) Estimator. By formulating a differentiable proxy for the discrete XOR logic, this module imposes a constraint during backpropagation. This design significantly increases the dependency of the generated key on the cover image features, making trivial identity mappings empirically unfavorable during optimization.

Second, to achieve robustness against screen-shooting, we devise a two-stage training strategy. Recognizing that screen-shooting noise creates a severe domain gap, we integrate a dedicated Restorer into the pipeline. By decoupling the logical binding learning from the physical restoration, this strat-

egy ensures that the model first learns the correct dependency and then adapts to the screen-shooting noise by recovering the image quality before decoding.

The main contributions of this paper are summarized as follows:

- We propose NiMark, the first end-to-end deep learning framework for non-intrusive watermarking robust against screen-shooting, effectively overcoming the bottlenecks of traditional hand-crafted features.
- We design the SG-XOR Estimator to enable gradient propagation through the discrete logical generation. This module enforces image-watermark binding by discouraging the network from converging to trivial structural shortcuts.
- We introduce a two-stage training strategy that integrates an independent restorer. This approach bridges the screen-shooting domain gap by rectifying distortions prior to decoding.
- Experiments demonstrate that NiMark achieves consistently stronger robustness over state-of-the-art methods, while maintaining zero visual distortion under the non-intrusive setting.

2 Related Work

2.1 Embedding-based Robust Watermarking

Traditional watermarking techniques operate in spatial or transform domains [Wolfgang *et al.*, 2002; Chu, 2003; Zhang and Wei, 2020; Liu and Tan, 2002] but struggle with non-linear distortions. Deep learning has transformed this field [Wu *et al.*, 2025], with end-to-end frameworks like HiDDeN [Zhu *et al.*, 2018] and subsequent refinements [Liu *et al.*, 2019; Jia *et al.*, 2021; Sander *et al.*, 2025]. Specifically for the screen-camera channel, early template matching [Fang *et al.*, 2018; Fang *et al.*, 2021] has been superseded by deep methods employing differentiable noise layers. StegaStamp [Tancik *et al.*, 2020] and PIMoG [Fang *et al.*, 2022] simulate perspective and Moiré distortions, while others explore inverse encoding [Wang *et al.*, 2025]. Recent works address geometric synchronization [He *et al.*, 2024], partial occlusion [Ma *et al.*, 2025; Chen *et al.*, 2025], and data-driven simulation [Wengrowski and Dana, 2019; Gao *et al.*, 2025; Wu *et al.*, 2026]. However, these methods inherently modify the cover image pixels to embed signals, which compromises visual fidelity and creates a bottleneck for applications requiring strict data integrity.

2.2 Non-Intrusive Watermarking and Shortcut Learning

Non-intrusive schemes [Wen *et al.*, 2003] construct logical verification keys to preserve image quality. Traditional algorithms rely on orthogonal moments [Gao and Jiang, 2015; Wang *et al.*, 2017] or their geometric invariants [Wang *et al.*, 2016; Wang *et al.*, 2019; Yang *et al.*, 2020; Yang *et al.*, 2021]. Recent studies have extended these to light fields [Wen *et al.*, 2025], Radon space [Qi *et al.*, 2024], and blockchain-based protocols [Wang *et al.*, 2022; Hou *et al.*, 2025]. Despite

ensuring zero distortion, these hand-crafted features lack robustness against severe screen-shooting attacks.

While deep learning approaches have emerged [Li *et al.*, 2025; Liu *et al.*, 2025], applying them to this task risks triggering shortcut learning [Geirhos *et al.*, 2020]. In general vision tasks, models tend to exploit superficial correlations such as background [Beery *et al.*, 2018], texture [Geirhos *et al.*, 2018], or high-frequency artifacts [Jo and Bengio, 2017; Smeu *et al.*, 2025]. However, the manifestation of this phenomenon in non-intrusive watermarking remains unexplored. In this work, we identify a domain-specific failure mode termed the Structural Shortcut, where the network completely bypasses the image-watermark binding to minimize loss. This critical vulnerability, which NiMark aims to resolve, represents a unique challenge distinct from previously studied shortcuts.

3 Methodology

Fig. 2 presents the NiMark framework. This section details four core components of the proposed watermarking system: the network architecture, the SG-XOR Estimator for enforcing logical binding, and a two-stage training strategy for handling screen-shooting distortions.

3.1 Network Architecture

The overall framework, shown in the top panel of Fig. 2, consists of four sequential modules: Encoder, Noise Layer, Restorer, and Decoder.

Encoder

The goal of the encoder is to generate a key from the cover image $I_{co} \in \mathbb{R}^{C \times H \times W}$ and a binary message $M \in \{0, 1\}^L$. To facilitate the interaction between the 1D message vector and the 2D image features, we design a dual-branch architecture. For the image feature extraction, we employ a differentiable moment feature extractor. We project the grayscale version of I_{co} onto a set of radial harmonic kernels defined in the polar coordinate system to directly extract a compact geometric feature map. Simultaneously, for the message branch, we employ a Message Processor. In this module, the message vector is first reshaped and then processed using convolution layers to match the spatial resolution of the extracted image features. Let $E(\cdot)$ denote the encoder. It fuses the normalized moment features with the processed message features to generate the encoded key $I_{en} \in \{0, 1\}^{C' \times H' \times W'}$, where C', H', W' denote the channel, height, and width of the feature maps, respectively.

$$I_{en} = E(I_{co}, M) \quad (1)$$

Noise Layer

In deep learning-based watermarking, the noise layer acts as a critical adversary during training. By accurately simulating real-world distortions, it drives the network to adaptively learn robust representations that can survive such attacks. Although our framework is non-intrusive, we follow this established strategy to acquire robustness. We integrate a differentiable noise layer $N(\cdot)$ to mimic the analog-to-digital screen-shooting process, comprising four key physical distortions:

a) Perspective Distortion: We apply a random 4-point perspective transformation matrix to simulate geometric deformation. **b) Lightness Distortion:** A linear brightness shift is applied defined as $I' = I + b$, where $b \sim U(0.5, 0.7)$. **c) Moiré Pattern:** We inject Moiré distortions generated using superimposed cosine functions with random orientations ($p = 0.2$). **d) Gaussian Noise:** Additive noise is introduced to simulate sensor grain.

In the non-intrusive setting, these distortions are applied directly to the cover image, denoted as $I_{no} = N(I_{co})$. It is worth noting that this module serves as a flexible component, which can be interchanged with distinct noise layers to target different attack scenarios.

Restorer

The Restorer, denoted as $R(\cdot)$, acts as a crucial preprocessing module to mitigate the domain gap. It aims to rectify the noise in the attacked image I_{no} to recover the visual content of the original cover. This restoration process is mathematically formulated as:

$$I_{re} = R(I_{no}) \quad (2)$$

where I_{re} represents the restored image. Ideally, $R(\cdot)$ learns the inverse transformation of the noise layer such that $I_{re} \approx I_{co}$, providing a cleaner reference for the subsequent decoding step.

Decoder

The Decoder $D(\cdot)$ extracts the watermark. In our non-intrusive setting, decoding is key-dependent. The decoder takes the generated encoded image I_{en} and the restored reference image I_{re} to retrieve the message:

$$M_{pre} = D(I_{en}, I_{re}) \quad (3)$$

The decoding process utilizes a Message Reverse Processing, which employs strided convolutions to downsample the feature maps back to the message dimension L .

3.2 Sigmoid-Gated XOR Estimator

A core component of our NiMark framework involves a hard binarization step using $\text{round}(\cdot)$ followed by a bitwise XOR operation. We explicitly design this module to force the model to learn a content-dependent watermark embedding. By inextricably linking the binarized image features with the binarized message features via XOR, the model is strongly encouraged to incorporate cover image features, as ignoring them leads to a clear performance degradation. This logical dependency explicitly reduces the tendency to converge to trivial structural shortcuts, ensuring a strong binding where the verification key is derived from the image features rather than being independent of the specific image content. The visual comparison of this discrete operation and our differentiable proxy is illustrated in Fig. 3.

In the forward pass, this operation is formally defined by the compound discrete function:

$$W = \text{round}(X_1) \oplus \text{round}(X_2) \quad (4)$$

where $X_1, X_2 \in [0, 1]^{C' \times H' \times W'}$ represent the pre-processed continuous feature tensors (feature maps). $\text{round}(\cdot)$ denotes

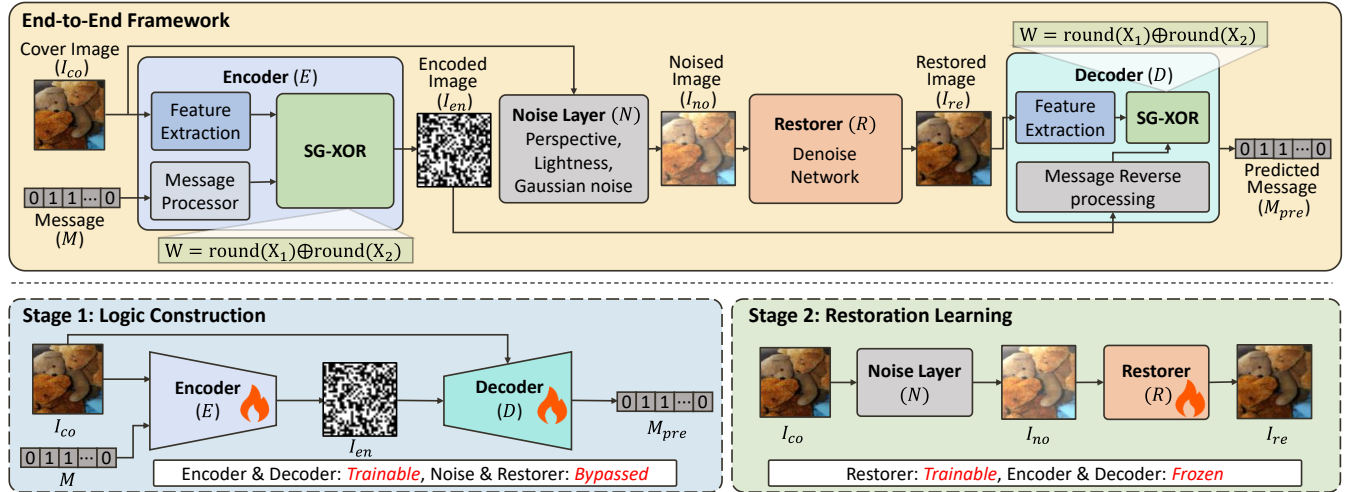


Figure 2: Overview of the proposed NiMark framework. The top panel illustrates the detailed network architecture which includes the Encoder integrated with SG-XOR, the Noise Layer, the Restorer, and the Decoder. The bottom panels demonstrate the proposed two-stage training strategy. Stage 1 constructs the logical dependency in a noise-free environment. Stage 2 independently optimizes the restoration network to handle screen-shooting distortions.

the element-wise hard binarization function, and \oplus is the element-wise logical XOR. The resulting discrete surface of W , as illustrated in Fig. 3a, exhibits sharp discontinuities and flat plateaus that block gradient flow, which poses a fundamental obstacle to gradient-based learning.

This operation is fundamentally non-differentiable. A common workaround, shown in Fig. 3b, is to use the Straight-Through Estimator (STE) [Bengio *et al.*, 2013], which simply copies gradients from the output to the input. Effectively, it treats the binarization as an identity function. However, the standard STE, which typically approximates the gradient of a binarization function as an identity map, i.e., a gradient of 1, is ill-suited for this complex, compound operation. Such a crude, linear approximation bears little resemblance to the highly non-linear gradient of the true $\text{round}(\cdot) \oplus \text{round}(\cdot)$ logic. This severe mismatch between the discrete forward pass and the oversimplified backward pass leads to unstable training and significant performance degradation.

To resolve this, we design a specialized, differentiable proxy gradient that accurately models the target discrete behavior. We term our approach the SG-XOR Estimator. The backward pass is derived from a composite proxy function that models the binarization, or gating, and the XOR logic operations. As shown in the workflow diagram (Fig. 4), we seek to find the gradients $\partial \mathcal{L} / \partial X_1$ and $\partial \mathcal{L} / \partial X_2$ during back-propagation.

Binarization Approximation

First, we approximate the non-differentiable $\text{round}(\cdot)$ function with a parameterized sigmoid function $\sigma_{m,n}(\cdot)$:

$$p_1 = \sigma_{m,n}(X_1) = \frac{1}{1 + \exp(-m(X_1 + n))} \quad (5)$$

$$p_2 = \sigma_{m,n}(X_2) = \frac{1}{1 + \exp(-m(X_2 + n))} \quad (6)$$

where p_1 and p_2 represent the soft binarization of X_1 and X_2 . This function is governed by two hyperparameters: the steepness parameter m and the binarization threshold n . The parameter m controls the sharpness of the sigmoid curve; we set $m = 10$ to enforce a close approximation to a step function. The parameter n defines the center of the transition. To accurately model the behavior of the $\text{round}(\cdot)$ function, which has its decision boundary at 0.5 for inputs in $[0, 1]$, we set the threshold to $n = -0.5$.

Continuous XOR Approximation

Next, we must define a continuous proxy for the discrete logic $p_1 \oplus p_2$. The target operation is defined by the XOR truth table. We select the bilinear polynomial that satisfies this condition, which is also equivalent to the probability of an XOR operation between two independent Bernoulli variables:

$$W_{\text{proxy}} = f(p_1, p_2) = p_1 + p_2 - 2p_1p_2 \quad (7)$$

This function aligns with the discrete XOR logic. For instance, at the input vertex $(1, 1)$, it yields $f(1, 1) = 1 + 1 - 2 = 0$, adhering to the truth table.

Gradient Computation

During the backward pass, we compute the gradient of the loss \mathcal{L} with respect to the original inputs X_1 and X_2 by applying the chain rule through our composite proxy function W_{proxy} . The detailed mathematical derivation and theoretical justification for this gradient flow are provided in the Supplementary Material. Here, we directly present the final gradients utilized for backpropagation, which are composed of a Logic Gradient and a Sigmoid Gate:

$$\frac{\partial \mathcal{L}}{\partial X_1} = \frac{\partial \mathcal{L}}{\partial W_{\text{proxy}}} \cdot \underbrace{(1 - 2p_2)}_{\text{Logic Gradient}} \cdot \underbrace{(m \cdot p_1(1 - p_1))}_{\text{Sigmoid Gate}} \quad (8)$$

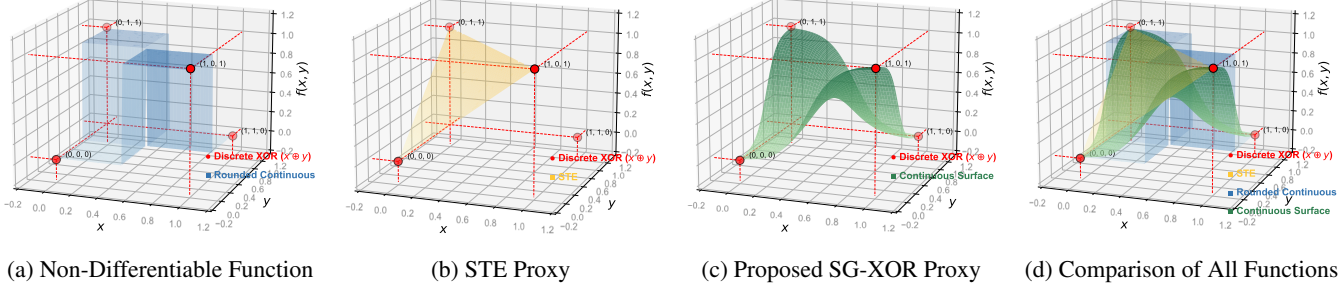


Figure 3: Visualization of the discrete XOR operation and its various differentiable proxies for gradient estimation. (a) The true, non-differentiable surface of the compound operation $W = \text{round}(X_1) \oplus \text{round}(X_2)$, which defines the discrete target behavior and causes gradient cliffs that prevent standard backpropagation. (b) The standard linear STE proxy, demonstrating a crude and misaligned gradient approximation. (c) The proposed SG-XOR proxy, providing a smooth, differentiable manifold that aligns well with the discrete XOR logic while maintaining differentiability. (d) Direct comparison among the SG-XOR proxy (green), STE proxy (yellow), and target discrete function (blue), showing the superior consistency of our approach.

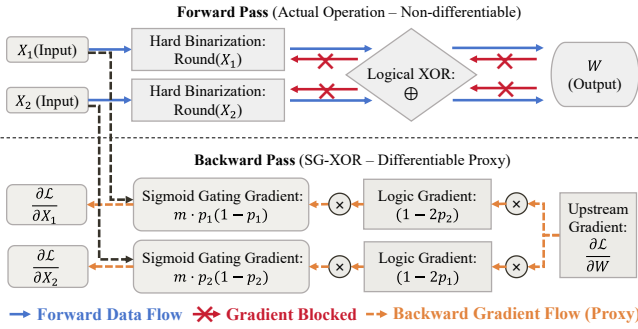


Figure 4: Mechanism of the proposed SG-XOR Estimator. The Forward Pass (top) performs the strict discrete operation $W = \text{round}(X_1) \oplus \text{round}(X_2)$, where gradients are naturally blocked by the hard binarization. The Backward Pass (bottom) utilizes our proposed differentiable proxy to estimate gradients. The upstream gradient is modulated by two distinct components: the Logic Gradient which enforces the XOR truth table and the Sigmoid Gating Gradient which stabilizes training near the decision boundaries.

$$\frac{\partial \mathcal{L}}{\partial X_2} = \frac{\partial \mathcal{L}}{\partial W_{proxy}} \cdot \underbrace{(1 - 2p_1)}_{\text{Logic Gradient}} \cdot \underbrace{(m \cdot p_2(1 - p_2))}_{\text{Sigmoid Gate}} \quad (9)$$

where $p_1 = \sigma_{m,n}(X_1)$ and $p_2 = \sigma_{m,n}(X_2)$ are re-computed during the backward pass using the saved inputs X_1 and X_2 . This formulation ensures both faithful approximation of the discrete logic and gradient-friendly learning dynamics.

3.3 Two-Stage Training Strategy

The specific data flows and component states for each training stage are visualized in the bottom panels of Fig. 2. Training deep networks directly under severe screen-shooting distortions is challenging due to the large domain gap. We propose a two-stage training strategy that decouples logical binding learning from physical restoration, ensuring the model captures both the correct dependency and robustness against noise.

Stage 1: Logic Construction

The primary goal of this stage is to construct the correct feature-watermark dependency via SG-XOR in a noise-free environment.

In this first stage, we bypass the noise layer and the restorer. The goal is to train the Encoder (E) and Decoder (D) to perform the fundamental non-intrusive watermarking task. The training is guided solely by the message recovery loss \mathcal{L}_{de} , as the visual quality of the cover image is naturally preserved in our non-intrusive setting. The decoder loss \mathcal{L}_{de} measures the error between the predicted message M_{pre} and the ground truth M :

$$\mathcal{L}_{stage1} = \mathcal{L}_{de} = \|M_{pre} - M\|_2^2 \quad (10)$$

where $\|\cdot\|_2^2$ denotes the Mean Squared Error (MSE). In this stage, the SG-XOR estimator enforces the logical binding. By learning to decode the message through the XOR operation, the network is forced to utilize the image features, thereby preventing the Structural Shortcut (identity mapping).

Stage 2: Restoration Learning

This stage aims to train the Restorer to rectify physical screen-shooting distortions independently.

In this second stage, we freeze the Encoder and Decoder. We focus exclusively on optimizing the Restorer (R). The network takes a distorted image and learns to recover the original cover:

$$I_{no} = N(I_{co}), \quad I_{re} = R(I_{no}) \quad (11)$$

The loss function \mathcal{L}_{stage2} enforces restoration quality using MSE and MS-SSIM:

$$\mathcal{L}_{stage2} = \lambda_{pix} \cdot \|I_{re} - I_{co}\|_2^2 + \lambda_{str} \cdot (1 - \text{SSIM}(I_{re}, I_{co})) \quad (12)$$

where we set $\lambda_{pix} = 10$ and $\lambda_{str} = 1$ to maintain consistent optimization objectives for pixel-level and structural fidelity. By recovering the image quality, the restorer effectively bridges the domain gap, allowing the pre-trained encoder and decoder from Stage 1 to function correctly even under attack conditions.

Method	Standard		Horizontal Perspective: Left				Horizontal Perspective: Right				Shooting Distance (Varying)					
	(0°, 30cm)		60°		30°		30°		60°		40cm		50cm		60cm	
	BER	U-BER	BER	U-BER	BER	U-BER	BER	U-BER	BER	U-BER	BER	U-BER	BER	U-BER	BER	U-BER
RHFM	21.10	24.24	22.62	22.75	20.38	22.98	20.56	23.29	19.74	23.16	21.23	22.86	21.04	24.08	21.13	23.85
EFM	19.24	20.40	19.91	20.67	18.23	20.95	18.64	20.76	18.55	20.36	19.01	19.97	19.44	20.60	19.63	21.22
PCET	20.04	20.91	20.44	22.03	19.16	21.33	19.82	21.38	18.91	20.32	20.25	21.07	20.55	21.76	20.52	21.86
BFM	20.51	22.66	21.90	22.85	19.82	21.85	20.18	22.40	19.85	23.45	20.70	23.53	20.42	23.54	21.16	22.60
FJFM	21.83	23.62	22.55	23.45	21.34	23.75	21.81	24.32	21.37	24.02	22.51	23.76	21.92	23.63	22.40	22.92
GPCET	19.26	20.69	19.39	20.93	18.25	20.70	19.05	20.28	17.96	20.50	19.57	21.09	19.77	20.42	19.66	21.23
FJFMR	8.58	9.68	8.70	9.36	8.36	9.77	8.40	9.58	8.38	8.73	8.42	9.27	8.47	9.22	8.65	9.42
GPCETR	14.94	16.31	16.08	17.15	14.91	16.61	14.98	17.70	14.69	16.31	15.37	16.08	15.15	16.81	15.32	15.62
GRHFMR	8.72	14.77	13.30	14.51	12.58	14.25	12.59	13.93	12.26	13.96	12.85	13.64	12.52	14.20	12.87	13.75
NiMark	0.46	49.41	1.13	53.82	0.97	40.25	0.68	48.16	1.28	47.32	0.57	51.98	0.58	51.64	0.59	51.03

Table 1: Robustness (BER %) and Binding Integrity (U-BER %) under varying horizontal angles and shooting distances. The “Standard” column denotes the baseline setting (0°, 30cm), while others vary a single parameter relative to this setting.

4 Experimentation

In this section, we evaluate the performance of NiMark. We first detail the experimental setup, then present comparisons against state-of-the-art methods, and finally validate our design choices through ablation studies.

4.1 Experimental Setup

Datasets and Implementation

Adhering to the protocol in [Wu *et al.*, 2024], we used 1,000 COCO images for training (with two disjoint test sets of 500 and 100 images) and employed the AdamW optimizer with a weight decay of 0.02 and a batch size of 16. Regarding the input configuration, consistent with [Wen *et al.*, 2025], we resized all images to 512 × 512 and set the message length to $L = 1024$ bits, yielding an encoded key I_{en} of size 1 × 32 × 32. The framework was implemented in PyTorch on an NVIDIA RTX 3060 GPU. The training followed our proposed two-stage strategy for a total of 300 epochs, regulated by a cosine annealing scheduler with a warmup period.

Baselines

To evaluate performance, we selected a comprehensive set of baselines.

1) Non-Intrusive Methods: We implemented 9 representative schemes based on orthogonal moments, including RHFM [Wang *et al.*, 2019], EFM [Wang *et al.*, 2016], PCET [Wang *et al.*, 2017], BFM [Gao and Jiang, 2015], FJFM [Yang *et al.*, 2021], GPCET [Yang *et al.*, 2020], FJFMR [Qi *et al.*, 2024], GPCETR [Qi *et al.*, 2024], and GRHFMR [Wen *et al.*, 2025]. 2) Screen-Shooting Resilient Methods: We compared NiMark against leading embedding-based frameworks designed for the screen-camera channel, including StegaStamp [Tancik *et al.*, 2020], PIMoG [Fang *et al.*, 2022], SRWSS [Gao *et al.*, 2025], SSDS [Li *et al.*, 2024] and S2R [Wu *et al.*, 2026].

Evaluation Metrics

1) Robustness: Measured by Bit Error Rate (BER, %). Lower is better.
 2) Visual Quality: Measured by PSNR (dB) and SSIM. For non-intrusive methods, the values are theoretically optimal (PSNR → ∞, SSIM = 1.0).

3) Unpaired BER (U-BER): To detect the Structural Shortcut, we verify whether the verification key is logically bound to the image content or has degenerated into a self-contained carrier. The U-BER evaluates the decoding performance when a specific valid key I_{en} is paired with incorrect, uncorrelated reference images. Crucially, to ensure the metric reflects the model’s behavior under attack conditions, the unpaired references undergo the exact same noise and restoration process as the correct cover. The U-BER for a single sample is calculated as the average error over K random unpaired references:

$$\text{U-BER} = \frac{1}{K} \sum_{k=1}^K \left(\frac{1}{L} \sum_{i=1}^L |m_i - D(I_{en}, I_{rand}^{(k)})_i| \right) \times 100\% \quad (13)$$

where $K = 10$ denotes the number of random reference images used for averaging to ensure stability, L is the message length, m_i is the i -th bit of the ground truth message, and $I_{rand}^{(k)}$ represents the k -th restored random reference image. Ideally, $\text{U-BER} \approx 50\%$, indicating that the key alone is insufficient for decoding without the correct image features.

4.2 Comparison with Non-Intrusive Schemes: Screen-Shooting Robustness

Table 1 presents the comprehensive evaluation results regarding horizontal perspective angles and varying shooting distances. Unless otherwise specified, experiments were conducted using a Lenovo Legion Y9000P display and a Samsung S20FE capture device, with a default setting of 30cm distance and a 0° angle (perpendicular to the screen). Results for vertical angles (Up and Down) are provided in the Supplementary Material.

As shown in Table 1, traditional moment-based methods exhibit instability under varying distances, with BERs fluctuating between 19% and 21%. In contrast, NiMark demonstrates superior robustness, maintaining BERs consistently below 3.5%. Crucially, NiMark achieves this while keeping U-BERs near 50% across all tested conditions, confirming that the logical binding is robustly preserved even under severe geometric distortions.

Method	PSNR	SSIM	Angle (Right) 30°	Distance 30cm
StegaStamp	33.07	0.904	1.27	1.13
PIMoG	36.06	0.967	8.27	6.94
SRWSS	33.98	0.963	22.97	12.4
S2R	42.27	0.962	6.68	3.51
NiMark	∞	1	0.68	0.46

Table 2: Comparison with SOTA screen-shooting resilient schemes. Robustness (BER %) vs. Visual Quality.

Display Device	Samsung S20 FE		iPhone 16		Vivo S17t	
	BER	U-BER	BER	U-BER	BER	U-BER
Lenovo Y9000P	0.46	49.41	0.73	49.43	0.62	51.89
Envision G249G	0.37	48.52	1.31	51.39	0.72	49.41
ASUS ROG Strix	1.06	47.92	0.88	50.80	0.47	50.31

Table 3: Cross-device robustness evaluation (BER % / U-BER %). The results demonstrate generalization across different display and capture hardware combinations.

4.3 Comparison with Non-Intrusive Schemes: Digital Attacks

To verify versatility, we also tested NiMark under standard digital attacks (JPEG, noise, filtering). Results provided in the Supplementary Material demonstrate that NiMark achieves competitive resilience, with U-BER consistently around 50%, confirming rigid logical binding.

4.4 Comparison with Screen-Shooting Resilient Schemes

We further compare NiMark with representative screen-shooting resilient methods: StegaStamp, PIMoG, SRWSS, and S2R. Table 2 presents the results regarding robustness and visual quality. Most baselines typically operate on 128×128 images with a 30-bit payload (≈ 0.0018 bpp). While S2R increases this to 64 bits (≈ 0.0039 bpp), NiMark processes 512×512 inputs with a 1024-bit message, maintaining a comparable bit density. Experimental results demonstrate that NiMark achieves strong robustness against screen-shooting. Furthermore, as a non-intrusive framework, it guarantees zero visual distortion, offering a viable alternative for scenarios requiring strict data integrity.

4.5 Cross-device Robustness Evaluation

To verify the generalization capability of NiMark across heterogeneous hardware, we conducted cross-device evaluations using a comprehensive test matrix involving three distinct display terminals (Lenovo Legion Y9000P, Envision G249G, ASUS ROG Strix SCAR Edition 8) and three different capture devices (Samsung Galaxy S20 FE, iPhone 16, Vivo S17t). This setup simulates real-world verification scenarios where the physical characteristics of screens and camera sensors vary significantly. Table 3 reports the BER performance for each hardware combination. The consistently low BERs across all pairings demonstrate NiMark’s generalization and stability across diverse hardware environments.

Module	Variant	BER (%)	U-BER (%)
Architecture	Cat + Conv Fusion	0.00	0.00
Gradient	STE	4.14	46.62
Noise Layer	StegaStamp	2.55	47.64
	PIMoG	1.26	50.53
	SSDS	1.96	47.36
	S2R	0.62	52.84
NiMark		0.46	49.41

Table 4: Ablation study on Architecture, Gradient Estimator, and Noise Layer.

Strategy	Description	BER (%)
S1 Only	Logic Pre-training	4.12
	Joint Training	0.68
NiMark	Two Stage	0.46

Table 5: Ablation study of training strategies. We compare our two-stage approach against logic-only pre-training and end-to-end joint training.

4.6 Ablation Studies

We investigate the effectiveness of key components in NiMark through controlled experiments. Table 4 summarizes the impact of architectural variants. First, replacing our SG-XOR with “Concat+Conv” fusion yields a near-zero U-BER, revealing that the key becomes self-contained; this explains the trivial 0% BER, as the model bypasses image features, rendering their distortion irrelevant. Furthermore, compared with the SG-XOR estimator, the variant using standard STE exhibits a much higher BER, as its oversimplified gradient fails to accurately model the discrete XOR logic. Finally, compared to noise layers from existing robust watermarking schemes (StegaStamp, PIMoG, SSDS, S2R), our noise layer achieves the best performance for the non-intrusive task, yielding the lowest BER of 0.46% under real-world attacks.

Impact of Training Strategy

Table 5 compares our two-stage strategy against single-stage baselines. Results indicate that: 1) Stage 1 Only: Training without the noise layer yields only limited robustness. 2) Joint Training: While end-to-end training is feasible, simultaneously optimizing for logical binding and restoration yields suboptimal robustness compared to our progressive strategy. 3) NiMark (S1 \rightarrow S2): By decoupling the two tasks, our strategy allows the network to focus on specific objectives at each stage, achieving the best overall robustness.

5 Conclusion

In this paper, we propose NiMark, a non-intrusive framework robust against screen-shooting. We identify the Structural Shortcut, a failure mode where networks may learn trivial identity mappings. To mitigate its impact, we introduce the SG-XOR estimator which bridges the non-differentiable gap. Furthermore, to bridge the severe domain gap caused by screen-shooting, we devise a two-stage training strategy that

decouples logic learning from physical restoration. Experiments demonstrate that NiMark achieves competitive and often superior robustness compared to state-of-the-art methods while maintaining zero visual distortion. Future work will focus on real-time mobile optimization and video protection.

References

[Beery *et al.*, 2018] Sara Beery, Grant Van Horn, and Pietro Perona. Recognition in terra incognita. In *Proc. Eur. Conf. Comput. Vis. (ECCV)*, pages 456–473, 2018.

[Bengio *et al.*, 2013] Yoshua Bengio, Nicholas Léonard, and Aaron Courville. Estimating or propagating gradients through stochastic neurons for conditional computation. *arXiv preprint arXiv:1308.3432*, 2013.

[Chen *et al.*, 2025] Mingyue Chen, Xin Liao, Han Fang, Jinlin Guo, Yanxiang Chen, and Xiaoshuai Wu. Flexible partial screen-shooting watermarking with provable robustness. *IEEE Trans. Circuits Syst. Video Technol.*, 2025.

[Chu, 2003] Wai C Chu. Dct-based image watermarking using subsampling. *IEEE Trans. Multimedia*, 5(1):34–38, 2003.

[Fang *et al.*, 2018] Han Fang, Weiming Zhang, Hang Zhou, Hao Cui, and Nenghai Yu. Screen-shooting resilient watermarking. *IEEE Trans. Inf. Forensics Secur.*, 14(6):1403–1418, 2018.

[Fang *et al.*, 2021] Han Fang, Dongdong Chen, Feng Wang, Zehua Ma, Honggu Liu, Wenbo Zhou, Weiming Zhang, and Nenghai Yu. Tera: Screen-to-camera image code with transparency, efficiency, robustness and adaptability. *IEEE Trans. Multimedia*, 24:955–967, 2021.

[Fang *et al.*, 2022] Han Fang, Zhaoyang Jia, Zehua Ma, Ee-Chien Chang, and Weiming Zhang. Pimog: An effective screen-shooting noise-layer simulation for deep-learning-based watermarking network. In *Proc. ACM Int. Conf. Multimedia (MM)*, pages 2267–2275, 2022.

[Gao and Jiang, 2015] Guangyong Gao and Guoping Jiang. Bessel-Fourier moment-based robust image zero-watermarking. *Multimed. Tools Appl.*, 74(3):841–858, 2015.

[Gao *et al.*, 2025] Guangyong Gao, Xiaoan Chen, Li Li, Zhihua Xia, Jianwei Fei, and Yun-Qing Shi. Screen-shooting robust watermark based on style transfer and structural re-parameterization. *IEEE Trans. Inf. Forensics Secur.*, 2025.

[Geirhos *et al.*, 2018] Robert Geirhos, Patricia Rubisch, Claudio Michaelis, Matthias Bethge, Felix A Wichmann, and Wieland Brendel. Imagenet-trained cnns are biased towards texture; increasing shape bias improves accuracy and robustness. 2018. *arXiv:1811.12231*.

[Geirhos *et al.*, 2020] Robert Geirhos, Jörn-Henrik Jacobsen, Claudio Michaelis, Richard Zemel, Wieland Brendel, Matthias Bethge, and Felix A Wichmann. Shortcut learning in deep neural networks. *Nature Machine Intelligence*, 2(11):665–673, 2020.

[He *et al.*, 2024] Mingjin He, Bingwen Feng, Yizhi Guo, Jian Weng, and Wei Lu. Camera-shooting resilient watermarking on image instance level. *IEEE Trans. Circuits Syst. Video Technol.*, 34(11):10874–10887, 2024.

[Hou *et al.*, 2025] Zhaoyang Hou, Haowen Yan, Liming Zhang, Na Ren, Rongjuan Ma, and Ruitao Qu. Zero-watermark method based on multi-channel PCNN and blockchain for remote sensing image transaction certificate and copyright protection. *IEEE Trans. Geosci. Remote Sens.*, 2025.

[Jia *et al.*, 2021] Zhaoyang Jia, Han Fang, and Weiming Zhang. Mbrs: Enhancing robustness of dnn-based watermarking by mini-batch of real and simulated jpeg compression. In *Proc. ACM Int. Conf. Multimedia (MM)*, pages 41–49, 2021.

[Jo and Bengio, 2017] Jason Jo and Yoshua Bengio. Measuring the tendency of CNNs to learn surface statistical regularities. In *arXiv preprint arXiv:1711.11561*, 2017.

[Li *et al.*, 2024] Yiyi Li, Xin Liao, and Xiaoshuai Wu. Screen-shooting resistant watermarking with grayscale deviation simulation. *IEEE Trans. Multimedia*, 2024.

[Li *et al.*, 2025] Jingyou Li, Rongle Wei, Xiaotian Xi, Guangda Zhang, Zixin Yang, and Fengshan Zhang. Dual-branch CNN-Transformer network for robust zero-watermarking of medical images. *Inf. Sci.*, page 122511, 2025.

[Liu and Tan, 2002] Ruizhen Liu and Tieniu Tan. An svd-based watermarking scheme for protecting rightful ownership. *IEEE Trans. Multimedia*, 4(1):121–128, 2002.

[Liu *et al.*, 2019] Yang Liu, Mengxi Guo, Jian Zhang, Yuesheng Zhu, and Xiaodong Xie. A novel two-stage separable deep learning framework for practical blind watermarking. In *Proc. ACM Int. Conf. Multimedia (MM)*, pages 1509–1517, 2019.

[Liu *et al.*, 2025] Xiyao Liu, Cundian Yang, Jianbiao He, Hui Fang, Gerald Schaefer, Jian Zhang, Yuesheng Zhu, and Shichao Zhang. Attack-defending contrastive learning for volumetric medical image zero-watermarking. *ACM Trans. Multimed. Comput. Commun. Appl.*, 21(2):1–23, 2025.

[Ma *et al.*, 2025] Zehua Ma, Han Fang, Xi Yang, Kejiang Chen, and Weiming Zhang. Ropass: Robust watermarking for partial screen-shooting scenarios. In *Proc. AAAI Conf. Artif. Intell. (AAAI)*, volume 39, pages 19332–19339, 2025.

[Qi *et al.*, 2024] Shuren Qi, Yushu Zhang, Chao Wang, Tao Xiang, Xiaochun Cao, and Yong Xiang. Representing noisy image without denoising. *IEEE Trans. Pattern Anal. Mach. Intell.*, 46(10):6713–6730, 2024.

[Sander *et al.*, 2025] Tom Sander, Pierre Fernandez, Alain Durmus, Teddy Furon, and Matthijs Douze. Watermark anything with localized messages. In *Int. Conf. Learn. Representations (ICLR)*, 2025.

[Smeu *et al.*, 2025] Stefan Smeu, Dragos-Alexandru Boldisor, Dan Oneata, and Elisabeta Oneata. Circumventing shortcuts in audio-visual deepfake detection datasets with unsupervised learning. In *Proc. IEEE/CVF Conf. Comput. Vis. Pattern Recognit. (CVPR)*, pages 18815–18825. IEEE, 2025.

[Tancik *et al.*, 2020] Matthew Tancik, Ben Mildenhall, and Ren Ng. Stegastamp: Invisible hyperlinks in physical photo-

tographs. In *Proc. IEEE Conf. Comput. Vis. Pattern Recognit. (CVPR)*, pages 2117–2126, 2020.

[Wang *et al.*, 2016] Chun-peng Wang, Xing-yuan Wang, Zhi-qiu Xia, Chuan Zhang, and Xing-jun Chen. Geometrically resilient color image zero-watermarking algorithm based on quaternion exponent moments. *J. Vis. Commun. Image Represent.*, 41:247–259, 2016.

[Wang *et al.*, 2017] Chun-peng Wang, Xing-yuan Wang, Xing-jun Chen, and Chuan Zhang. Robust zero-watermarking algorithm based on polar complex exponential transform and logistic mapping. *Multimed. Tools Appl.*, 76(24):26355–26376, 2017.

[Wang *et al.*, 2019] Chunpeng Wang, Xingyuan Wang, Zhiqiu Xia, and Chuan Zhang. Ternary radial harmonic Fourier moments based robust stereo image zero-watermarking algorithm. *Inf. Sci.*, 470:109–120, 2019.

[Wang *et al.*, 2022] Baowei Wang, Jiawei Shi, Weishen Wang, and Peng Zhao. Image copyright protection based on blockchain and zero-watermark. *IEEE Trans. Netw. Sci. Eng.*, 9(4):2188–2199, 2022.

[Wang *et al.*, 2025] Heng Wang, Hongxia Wang, Fei Zhang, Zhenhao Shi, and Xinyi Huang. Moiré-watermark: Robust watermarking against screen-shooting using moiré patterns. *IEEE Trans. Multimedia*, 2025.

[Wen *et al.*, 2003] Quan Wen, T-F Sun, and S-X Wang. Concept and application of zero-watermark. *Acta Electron. Sin.*, 31(2):214–216, 2003.

[Wen *et al.*, 2025] Wenying Wen, Yu Ye, Ziye Yuan, Baolin Qiu, and Dingli Hua. LFIZW-GRHFMR: Robust zero-watermarking with GRHFMR for light field image. *ACM Trans. Multimed. Comput. Commun. Appl.*, 21(4):1–17, 2025.

[Wengrowski and Dana, 2019] Eric Wengrowski and Kristin Dana. Light field messaging with deep photographic steganography. In *Proc. IEEE Conf. Comput. Vis. Pattern Recognit. (CVPR)*, pages 1515–1524, 2019.

[Wolfgang *et al.*, 2002] Raymond B Wolfgang, Christine I Podilchuk, and Edward J Delp. Perceptual watermarks for digital images and video. *Proc. IEEE*, 87(7):1108–1126, 2002.

[Wu *et al.*, 2024] Yufeng Wu, Baowei Wang, Guiling Wang, and Xin Liao. Mcfn: Multi-scale crossover feed-forward network for high performance watermarking. *Neurocomputing*, page 129282, 2024.

[Wu *et al.*, 2025] Shaowu Wu, Wei Lu, and Xiangyang Luo. Robust watermarking based on multi-layer watermark feature fusion. *IEEE Trans. Multimedia*, 2025.

[Wu *et al.*, 2026] Yufeng Wu, Xin Liao, Baowei Wang, Han Fang, Xiaoshuai Wu, Mingyue Chen, and Guiling Wang. Sim-to-real: An unsupervised noise layer for screen-camera watermarking robustness. In *Proc. AAAI Conf. Artif. Intell. (AAAI)*, volume 40, 2026.

[Yang *et al.*, 2020] Hong-ying Yang, Shu-ren Qi, Pan-pan Niu, and Xiang-yang Wang. Color image zero-watermarking based on fast quaternion generic polar complex exponential transform. *Signal Process. Image Commun.*, 82:115747, 2020.

[Yang *et al.*, 2021] Hongying Yang, Shuren Qi, Jialin Tian, Panpan Niu, and Xiangyang Wang. Robust and discriminative image representation: Fractional-order Jacobi-Fourier moments. *Pattern Recognit.*, 115:107898, 2021.

[Zhang and Wei, 2020] Lina Zhang and Deyun Wei. Image watermarking based on matrix decomposition and gyrator transform in invariant integer wavelet domain. *Signal Process.*, 169:107421, 2020.

[Zhu *et al.*, 2018] Jiren Zhu, Russell Kaplan, Justin Johnson, and Li Fei-Fei. Hidden: Hiding data with deep networks. In *Proc. Eur. Conf. Comput. Vis. (ECCV)*, pages 657–672, 2018.